Au@TiO_2-CdS Ternary Nanostructures for Efficient Visible-light-Driven Hydrogen Generation

Jun Fang[a], *Lin Xu*[a], *Zhenyi Zhang*[a], *Yupeng Yuan*[a], *Shaowen Cao*[a], *Zheng Wang*[a], *Lisha Yin*[a], *Yusen Liao*[a], *and Can Xue*[a,]*

[a] Solar Fuels Laboratory, School of Materials Science and Engineering, Nanyang Technological University, 50 Nanyang Avenue, Singapore 639798 ,Singapore

*__Corresponding Author__. Tel.: +65- 6790 6180;

E-mail: cxue@ntu.edu.sg

ABSTRACT: We report a new type of Au@TiO_2-CdS ternary nanostructures by decorating CdS nanoparticles onto Au@TiO_2 core-shell structures. Comparing to the binary structures, such as CdS-TiO_2 and Au@TiO_2, these ternary nanostructures exhibit remarkably high photocatalytic H_2 generation rate under visible-light irradiation. The enhanced photocatalytic activity is attributed to the unique ternary design, which builds up a transfer path for the photoexcited electrons of CdS to the core Au particles via the TiO_2 nanocrystal bridge, and thus effectively suppressed the electron-hole recombination on the CdS photocatalyst. This internal electron transfer pathway (CdS→TiO_2→Au) eliminates the needs of post-deposition of metal co-catalyst since the core Au nanoparticle can act as the interior active catalyst for proton reduction towards hydrogen evolution. We believe that our work demonstrates a promising way for rational design of metal-semiconductor hybrid photocatalysts to achieve high photocatalytic efficiency for solar fuels production.

TOC Graphic

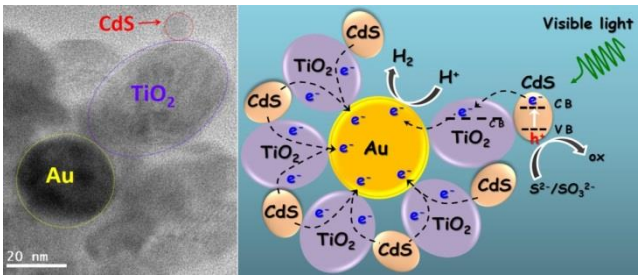

KEYWORDS: Au particles, TiO_2, CdS, ternary nanostructure, H_2 generation, efficient electron transfer

1. INTRODUCTION

In the past decade hydrogen fuel has been attracting more and more attentions as one of the promising clean energy sources as oppose to conventional fossil fuels.[1] Photocatalytic H_2 evolution over inorganic semiconductors under visible light illumination has been widely explored as a potential avenue for solar fuels production.[2-4] In particular, TiO_2 as one of the typical photocatalysts has been extensively studied over a few decades due to its low cost, non-toxicity and high chemical stability.[5-8] However, the wide band gap (>3.2 eV) of TiO_2 restricts its utilization of the visible light in the solar spectrum, and the high recombination rate of photogenerated electrons and holes in TiO_2 often leads to low quantum yield and poor photocatalytic activity.[9] Recent studies have demonstrated that combining the wide band gap photocatalyst with smaller band gap semiconductors, such as metal chalcogenides, would be an effective way to harvest visible light and promote charge separation towards high photocatalytic efficiency for H_2 generation.[10-15] Among the small band gap semiconductors, CdS is an excellent candidate due to its ideal band gap (2.4eV) and band edge levels that are capable of driving both reduction and oxidation of water under visible light irradiation. It has been reported that the CdS-TiO_2 composites could show better photostability and photocatalytic activities than either individual component.[16-19]

Nevertheless, in order to apply the CdS-TiO_2 composites for H_2 generation, deposition of noble metal co-catalyst (e.g. Pt or Au) onto the composites is usually required to lower down the overpotential for hydrogen evolution.[20-23] In general, loading of metal co-catalysts allows rapid interfacial electron transfer from excited semiconductors to the metal co-catalysts, which retards recombination of photogenerated electron-hole pairs and thereby promote the photocatalytic efficiency. Conventionally, post-deposition of metal nanoparticles onto semiconductor surfaces

could be achieved through photodeposition or co-precipitate with calcination or reduction.[24] However, in case of binary semiconductor composite, for example CdS-TiO_2, the post-deposition method usually leads to random loading of metal nanoparticles onto the surfaces of both TiO_2 and CdS. Since the conduction band level of CdS is higher than that of TiO_2, in the visible-light-driven photocatalytic process of proton reduction into H_2, the photoexcited electrons in CdS conduction band could rapidly transfer to TiO_2 conduction band through the CdS-TiO_2interfaces. As such, the effective proton reduction would have to occur on TiO_2 surfaces. In order to promote the H_2 evolution on TiO_2 surface, it would be desirable to have selective deposition of metal co-catalysts on TiO_2 surfaces rather than random loading onto both CdS and TiO_2 surfaces, in which the metal co-catalysts sitting on CdS surfaces would become waste and may act as the charge recombination centers with decreasing the overall photocatalytic efficiency of CdS-TiO_2 composites.

Herein, we present the preparation of ternary Au@TiO_2-CdS nanostructures in which CdS nanoparticles are decorated on the outer surfaces of Au@TiO_2 core-shell structures. This rationally constructed ternary structure builds up a transfer path for the visible-light-excited electrons of CdS to the core Au particles via the TiO_2 nanocrystal bridge. This internal electron transfer pathway (CdS→TiO_2→Au) eliminates the needs of post-deposition of metal co-catalyst because the core Au nanoparticle is not fully covered by the TiO_2 nanocrystal shell, and thereby can act as the interior active co-catalyst for proton reduction towards hydrogen generation. As a result, this ternary Au@TiO_2-CdS structure exhibit significantly improved visible-light-driven activity for photocatalytic H_2 generation as compared to the binary structures such as CdS-TiO_2 and Au@TiO_2. We believe that our study points out a promising way for rational design of ternary nanostructures of metal-semiconductor hybrids to achieve high efficiency for

photocatalytic solar fuels production.

2. EXPERIMENTAL SECTION

2.1 Sample preparation

Seed growth of 40nm gold nanoparticles: Firstly, the 15-nm gold nanoparticle seeds were synthesized by rapidly injecting an aqueous solution of trisodium citrate (5mL, 38.8mM) into a boiling aqueous solution of $HAuCl_4$ (50mL, 1mM) under vigorous stirring. After the solution color changed to wine red, heating was removed to allow the solution cooling down to room temperature. This solution is referred as the colloid of 15-nm gold nanoparticle seeds. For the preparation of 40-nm gold nanoparticles, in a typical procedure, an aqueous solution of $HAuCl_4$ (125 mL, 0.25mM) was heated and kept boiling under vigorous stirring. Then 1.125 mL colloid solution of pre-synthesized 15-nm Au seeds and 0.56 mL aqueous solution of sodium citrate (38.8mM) were injected into the above solution. After the solution turned into wine red, 5 mL solution of sodium citrate (38.8mM) was added into the solution as the extra stabilizer, and the mixture was kept boiling for another 30 min.

Shell growth of TiO_2 on the Au nanoparticles: The growth of TiO_2 nanocrystal shell on the 40-nm Au nanoparticle was achieved through a hydrothermal process according to literature protocols.[25] Typically, 36 mL solution of the as-prepared 40-nm Au nanoparticles was mixed with 4.5 mL aqueous solution of TiF_4 (40 mM). The mixture was kept stirring for 30 min, then diluted to 80mL with deionized water and transferred into a 100-mL Teflon-lined stainless steel autoclave that was subsequently treated at 180^{o}C for 24 h. After that, the product was cooled down to room temperature, centrifuged and washed with the deionized water for several times.

Decorating CdS nanoparticles onto Au@TiO_2 core-shell structures: The calculated amount of $Cd(CH_3COO)_2 \cdot 2H_2O$ was added into 10 mL aqueous suspension of the Au@TiO_2 core-shell

structures. Then 50μL thioglycolic acid was added into the above suspension under stirring. Stoichiometric amount of Na_2S was followed introduced into the afore-mentioned suspension. The suspension was then transferred into a 40-mL Teflon-lined stainless steel autoclave that was subsequently treated at 160^oC for 10h. The product was cooled down to room temperature, centrifuged, washed with deionized water for several times, and dried at 60^oC in air. The final sample is denonted as Au@TiO_2-xCdS, in which x refers to the molar ratio of CdS to TiO_2. (For instance, x=0.1 means CdS:TiO_2 is 10% in molar ratio.)

2.2 Sample Charaterization

The crystalline phases of the samples were examined by powder X-ray diffraction (XRD) on a Shimazu XRD-6000 X-ray diffractometer (Cu K_α irradiation source) with the scanning speed of 2^o/min in the 2θ range of 20^o to 80^o. UV-vis diffuse reflectance spectra were acquired on a Lambda 750 UV/Vis/NIR spectrophotometer (Perkin Elmer, USA). The sample morphology was examined by field-emission scanning electron microscopy (SEM, JEOL JSM-7600F) with energy-dispersive X-ray (EDX) analysis system and transmission electron microscopy (TEM, JEOL JEM-2010) with an accelerating voltage at 200 kV.

2.3 Photocatalytic reduction of water for H_2 evolution

In a typical run, 2 mg Au@TiO_2-xCdS photocatalysts were suspended in 10 mL aqueous solution containing 0.25 M Na_2S and 0.35 M Na_2SO_3 as the sacrificial agents. The suspension was sealed in a quartz vessel and purged with Argon for 30 min to drive away the residual oxygen. After degassing, the vessel was exposed under a 300-W Xenon lamp (MAX-302, Asahi Spectra Co. Ltd.) coupled with a UV cutoff filter (λ>420 nm) to evaluate the photocatalytic activity under visible light irradiation. The gas products were analyzed periodically by an Agilent 7890A gas chromatograph (GC) with a thermal conductivity detector (TCD). For the

photocatalytic test under irradiation at a specific wavelength (420 nm or 550 nm), the experimental settings are identical as the above description except that the UV cutoff filter (λ>420 nm) was replaced by the band pass filter (420±10 nm or 550±20 nm).

3. RESULTS AND DISCUSSION

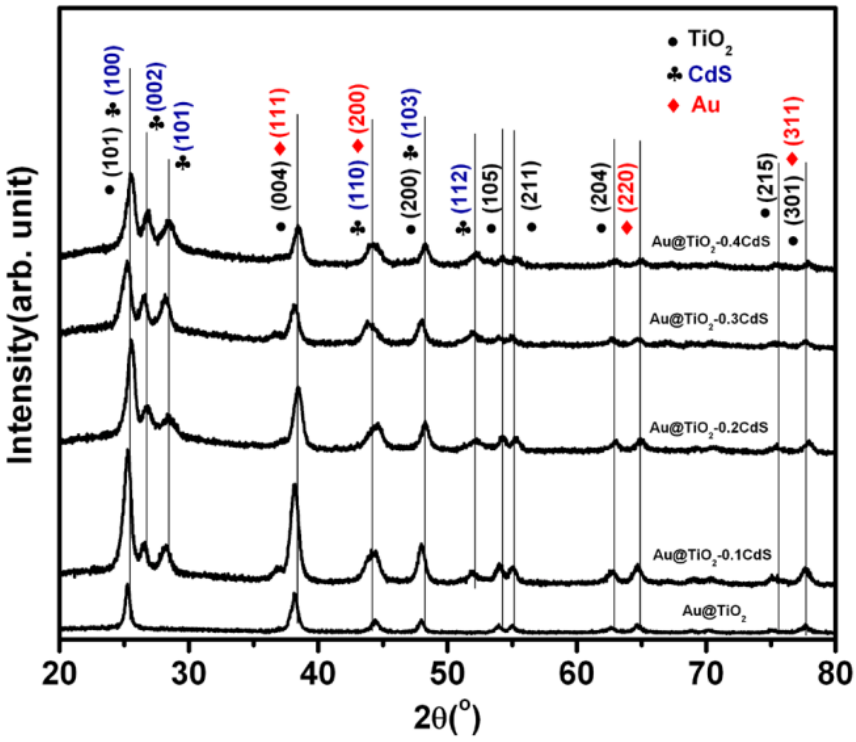

Figure 1. XRD patterns of various Au@TiO_2-CdS nanocomposites.

The XRD patterns of Au@TiO_2 and various Au@TiO_2-CdS samples with different CdS loading amount were shown in Figure 1. For the Au@TiO_2 nanocomposite, we can observe the characteristic diffraction peaks of anatase TiO_2 (JCPDS card No. 83-2243) and face-centered cubic (FCC) Au (JCPDS card No. 01-1174). Note that the TiO_2 (004) peak at 38.2^o is overlapping with Au (111) peak at the same 2θ degree. Upon decoration with CdS nanoparticles, the XRD patterns exhibit characteristic peaks of hexagonal CdS (JCPDS card No. 41-4019). The CdS (110) peak at 43.9^o has some overlap with Au (200) peak at 44.4^o. All peaks from the

sample before CdS decoration remained there, indicating the secondary hydrothermal process did not influence the phases of original Au@TiO_2 structures. In short, the final ternary structures contain three phases, FCC Au, anatase TiO_2 and hexagonal CdS.

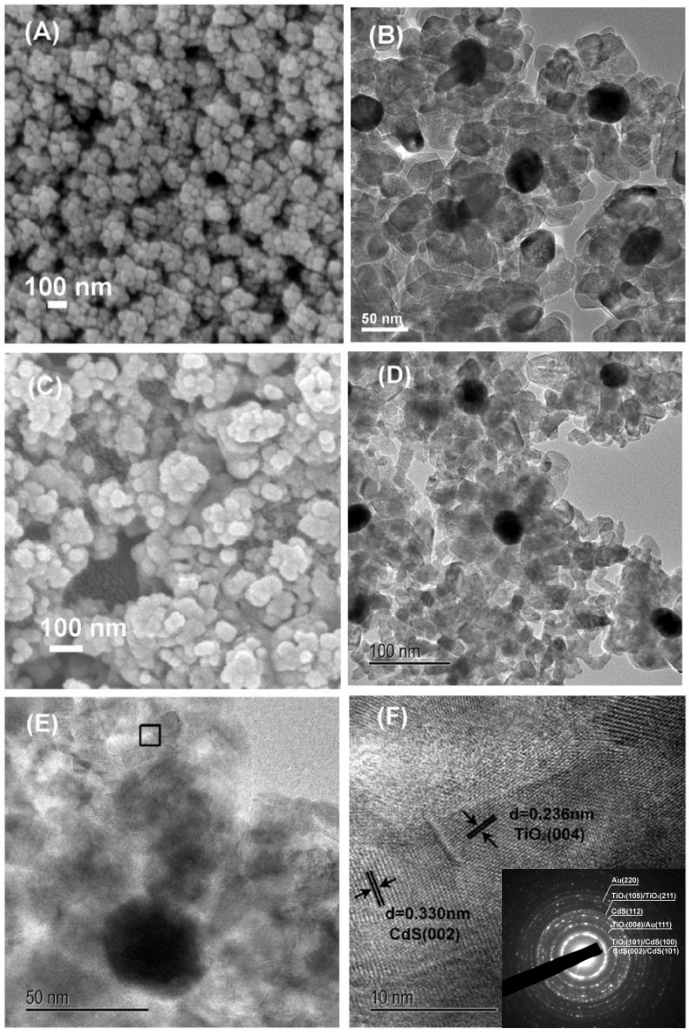

Figure 2. SEM and TEM images of the as-prepared Au@TiO_2-CdS nanocomposites. (A) SEM image of Au@TiO_2; (B) TEM image of Au@TiO_2; (C) SEM image of Au@TiO_2-0.2CdS; (D) and (E) TEM images of Au@TiO_2-0.2CdS; (F) HRTEM image of Au@TiO_2-0.2CdS. The inset of (F) is SAED patterns of Au@TiO_2-0.2CdS.

The Au@TiO_2 core-shell structure was confirmed by TEM and SEM. As shown in Figure 2A

and 2B, the 40-nm Au nanoparticles were all encapsulated in TiO_2 nanocrystal shells, forming flower- like spherical structures with an average diameter of ~120nm. The molar ratio of Au to TiO_2 was estimated as ~5% according to the EDX analysis (Figure S2). After the secondary hydrothermal process for CdS decoration, such flower-like structures were well preserved, as shown in Figure 2C , 2D and S1. We can observe CdS nanoparticles (10~20 nm) appearing on the outer surface of TiO_2 nanocrystal shells, and the density of CdS particles became higher as the ratio of CdS to TiO_2 increases. The EDX analysis (Figure S2) confirm that for all Au@TiO_2-xCdS samples, the actual CdS to TiO_2 ratio is fairly close to the theoretically calculated ratio based on the precursor concentrations. The HRTEM images (Figure 2E and 2F) reveal that the CdS nanoparticles are intimately contacted with the TiO_2 nanocrystal shells with clear CdS-TiO_2 interfaces. In Figure 2F, we can observe a lattice spacing of 0.236 nm corresponding to (004) facet of anatase TiO_2, and another lattice spacing of 0.330 nm corresponding to (002) facet of hexagonal CdS. The selected area electron diffraction (SAED) pattern is shown in the Figure 2F inset. The labels from lower position to upper ones are TiO_2(101)/CdS(100)/CdS(002)/CdS(101), TiO_2(004)/Au(111), CdS(112), TiO_2(105)/TiO_2(211) and Au(220), respectively, which is in agreement with the XRD results.

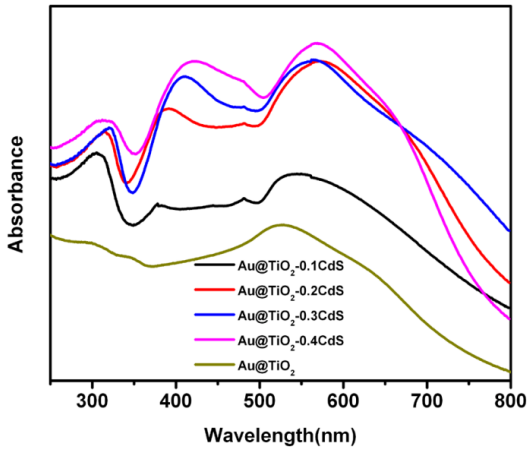

Figure 3. UV-vis diffuse reflectance spectra of various Au@TiO_2-CdS samples.

Figure 3 shows the absorption spectra of the Au@TiO_2-xCdS ternary nanostructures. The UV absorption band at ~320 nm could be attributed to the band edge absorption of anatase TiO_2.[26] The absorption features from 360 to 520nm arise from band absorption of CdS nanoparticles.[27] Based on the XRD results, the crystalline sizes of CdS particles were calculated as 12.1, 8.27, 12.0, 10.0 nm for Au@TiO_2-0.1CdS, Au@TiO_2-0.2CdS, Au@TiO_2-0.3CdS, Au@TiO_2-0.4CdS, respectively. Moreover, this CdS absorption band red shifts with higher loading amount of CdS, which might be due to the aggregation of the CdS nanoparticles into larger domains.[27] The absorption features from 530 to 580 nm come from the surface plasmon resonance (SPR) characteristic of the 40-nm Au nanoparticles encapsulated in the TiO_2 shells.[28]

It is notable that the Au SPR absorption peak shows a red-shift from 530nm (Au@TiO_2) to 570 nm (Au@TiO_2-0.4CdS). This implies that in the Au@TiO_2 core-shell structure, the TiO_2 nanocrystalline shell may not fully cover the entire surface of the Au nanoparticle core, thus in the hydrothermal process of CdS decoration on the Au@TiO_2 structure, some CdS could directly deposit on the Au nanoparticle surface,[29] as evidenced by the HRTEM observation (Figure S3). As is well known, the SPR wavelength of a gold nanoparticle is highly sensitive to the dielectric environment near its surface,[30] as such, the higher dielectric constant of CdS (vs. air) and direct contact of deposited CdS with Au nanoparticle surface would lead to red-shift of the Au SPR band. In order to further verify this hypothesis, we performed an etching treatment on the Au@TiO_2-0.2CdS sample by using HCl solution to remove the deposited CdS. The absorption spectra (Figure S4) showed that the peak attributed to CdS attenuated sharply and the SPR wavelength of Au nanoparticles retreated from 570nm to 545nm after HCl etching. This confirms the influence of deposited CdS on the Au SPR absorption features.

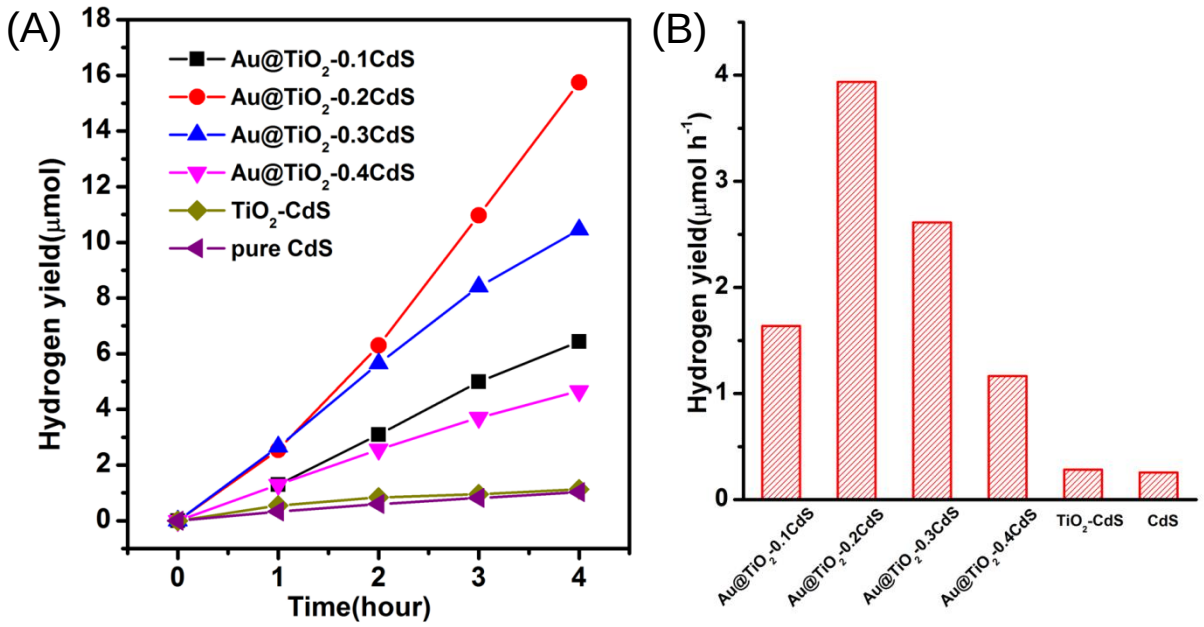

Figure 4. (A) Plots of photocatalytic H_2 evolution amount versus visible light irradiation (λ>420 nm) time by various samples; (B) The H_2 evolution rate by various samples.

The ternary Au@TiO_2-xCdS nanostructures were used for photocatalytic H_2 generation under visible light (λ>420 nm) irradiation in the aqueous electrolyte solution containing 0.25M Na_2S and 0.35M Na_2SO_3, which act as the sacrificial agents to quench the holes. For comparison, control samples of pure CdS nanoparticles and the TiO_2-0.2CdS nanocomposite without Au cores were also prepared (see supporting info for details). As shown in Figure 4, we observed very weak photocatalytic activity in H_2 generation for both pure CdS (0.25 μmol•h^{-1}) and TiO_2-0.2CdS (0.28 μmol•h^{-1}) samples. Significantly, in the presence of Au nanoparticle cores, the ternary Au@TiO_2-0.2CdS sample exhibit more than 10 times higher activity (3.94 μmol•h^{-1} catalyst) as compared to the TiO_2-0.2CdS sample without Au cores. The remarkable enhancement of photocatalytic activity could be attributed to the unique design of ternary Au@TiO_2-CdS structures that allow efficient CdS→TiO_2→Au pathway for electron transfer, as

illustrated in Figure 5. Upon light excitation, active electrons are generated in the CdS conduction band, and then rapidly injected into the conduction band of contacted TiO_2, which serves as a bridge to transport these electrons to the Au core. It is known that the Au nanoparticle can act as electron trap in the photocatalytic process to promote the separation of photogenerated charge carriers.[31] Thereby, the Au cores in this ternary structure could capture and store the photoexcited electrons from CdS nanoparticles on the TiO_2 shells to induce proton reduction for H_2 evolution on the Au surface, while the photogenerated holes remaining on CdS could be quenched by the sulfide ions in the solution. It is believed that this internal ($CdS \rightarrow TiO_2 \rightarrow Au$) electron transfer process effectively suppressed the electron-hole recombination on CdS, and thereby significantly enhanced the photocatalytic H_2 generation rate.

The direct contribution of photocatalytic activity from Au SPR excitation could be excluded because the Au@TiO_2 core-shell sample before CdS decoration showed extremely low H_2 generation rate (0.001 $\mu mol \bullet h^{-1}$, not shown in Figure 4 as it is too low). This suggests that the CdS nanoparticles could be considered as the sole visible-light absorber to induce photocatalytic activity. Consistently, we observed 2.4 times increased H_2 generation rate when the CdS loading ratio increases from the Au@TiO_2-0.1CdS sample (1.64 $\mu mol \bullet h^{-1}$) to the Au@TiO_2-0.2CdS sample (3.94 $\mu mol \bullet h^{-1}$). However, it was found that further increasing the CdS decoration amount led to lower photocatalytic activity, which is evidenced by the decreased H_2 generation rate for the Au@TiO_2-0.3CdS sample (2.61 $\mu mol \bullet h^{-1}$) and the Au@TiO_2-0.4CdS sample(1.16 $\mu mol \bullet h^{-1}$). This could be attributed to two reasons. First, the overloading of CdS onto Au@TiO_2 structures might retard the proton diffusion through the internal vacancies within the ternary structure, which could reduce the photocatalytic activity of proton reduction. Second, the higher precursor concentration for more CdS loading might result in aggregation of CdS nanoparticles

on the TiO_2 shells as evidenced by Figure S1F, and such an aggregation of CdS particles created grain boundaries that would trap charge carriers during the charge transfer process to decline the photocatalytic reactions.

It has been reported that the SPR of Au nanoparticles could also enhance the charge separation of nearby semiconductors through plasmon-exciton coupling, and thereby promote photocatalytic performance.[28] For our ternary Au@TiO_2-CdS structures, in order to verify whether the SPR of Au cores contributes to the enhanced H_2 generation rate, we carry out additional photocatalytic tests by using the Au@TiO_2-0.2CdS sample with control of irradiation wavelengths. In a control experiment, under the light irradiation at 420±10 nm which only excites CdS nanoparticles, there was apparent H_2 evolution with a rate 0.1 $\mu mol \bullet h^{-1}$ (corresponding to a quantum yield of 0.55%). However, when we simultaneously introduced a secondary irradiation at 550±20 nm which excites the SPR of Au cores, no enhancement on the H_2 generation rate was observed. This means that the SPR excitation of Au cores could not provide significant contribution to the photocatalytic activity of the ternary Au@TiO_2-CdS nanostructures.

The stability of the photocatalyst was also evaluated through recycling test of photocatalytic H_2 evolution by using the Au@TiO_2-0.2CdS structure. As shown in Figure S6, after three cycles, the photocatalytic H_2 generation rate still can maintain 90% of the original activity as compared to the first cycle, suggesting the good stability of the Au@TiO_2-0.2CdS. Nevertheless, the 10% drop of the activity suggests that photo-corrosion of CdS particles may still occur during the photocatalytic reactions.

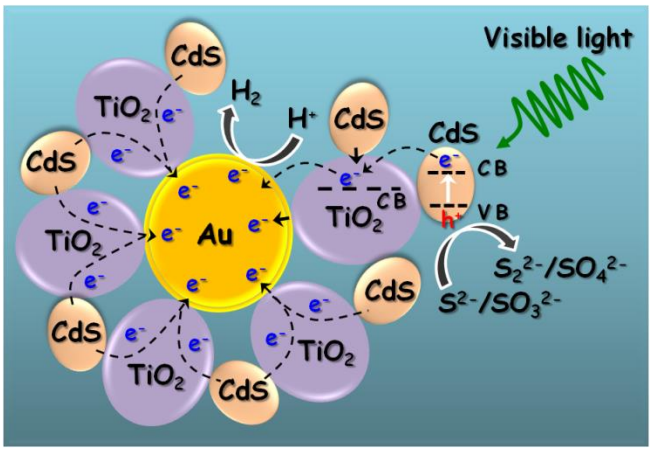

Figure 5. Schematic illustration of photocatalytic H_2 generation by Au@TiO_2-CdS ternary nanostructures under visible light irradiation.

4. CONCLUSIONS

The ternary Au@TiO_2-CdS nanostructures were successfully constructed through decoration of CdS nanoparticles onto Au@TiO_2 core-shell structures. This ternary design builds up a transfer path for the photoexcited electrons of CdS to the core Au particles via the TiO_2 nanocrystal bridge, and thus effectively suppressed the electron-hole recombination on the CdS photocatalyst. As such, these ternary nanostructures exhibit remarkably high photocatalytic H_2 generation rate under visible-light irradiation comparing to the binary structures, such as CdS-TiO_2 and Au@TiO_2. This internal electron transfer pathway (CdS→TiO_2→Au) eliminates the needs of post-deposition of metal co-catalyst since the core Au nanoparticle can act as the interior active co-catalyst for proton reduction towards hydrogen evolution. We believe that our work demonstrates a promising way for rational design of metal-semiconductor hybrid photocatalysts to achieve high photocatalytic efficiency for solar fuels production.

ACKNOWLEDGMENTS

This work is financially supported by NTU Start-Up Grant (SUG), NTU seed funding for Solar Fuels Laboratory, MOE AcRF-Tier1 RG 44/11, MOE AcRF-Tier 2 (MOE2012-T2-2-041, ARC 5/13), and CRP (NRF-CRP5-2009-04) from NRF Singapore.

ASSOCIATED CONTENT

Supporting Information Available

Synthesis methods of CdS nanoparticles and TiO_2-0.2CdS nanocomposite without Au cores, the method of etching CdS nanoparticles to re-obtain Au@TiO_2 core-shell structure, SEM and TEM images of as-prepared Au@TiO_2-CdS nanocomposites, EDX analysis of various Au@TiO_2-CdS nanocomposites, UV-Vis diffuse reflectance spectra of Au@TiO_2-0.2CdS before and after 3M HCl etching, TEM images of TiO_2-0.2CdS and pure CdS catalysts, Recycling photocatalytic H_2 evolution test by Au@TiO_2-0.2CdS, Band energy diagram for the Au@TiO_2-CdS ternary structure. This information is available free of charge via the Internet at http://pubs.acs.org/**.**

REFERENCES

(1) Penner, S.S. *Energy* **2006**, 31, 33-43.

(2) Chen, X. B.; Shen, S. H.; Guo, L. J.; Mao, S. S. *Chem. Rev.* **2010**, 110, 6503-6570.

(3) Kudo, A.; Miseki, Y. *Chem. Soc. Rev.* **2009**, 38, 253-278.

(4) Kubacka, A.; García, M. F.; Colón, G. *Chem. Rev.* **2012**, 112, 1555-1614.

(5) Fujishima, A.; Honda, K. *Nature* **1972**, 238, 37-38.

(6) Thompson, T. L.; Yates, J. T. *Chem. Rev.* **2006**, 106, 4428-4453.

(7) Antony, R. P.; Mathews, T.; Ramesh, C.;Murugesan, N.; Dasgupta, A.; Dhara, S.; Dash, S.; Tyagi, A. K. *Int. J. Hydrogen Energy* **2012**, 37, 8268-8276.

(8) Fang, J.; Cao, S. W.; Wang, Z.; Shahjamali, M. M.; Boey, F.; Loo, S. C. J.; Barber, J.; Xue, C. *Int. J. Hydrogen Energy* **2012**, 37, 17853-17861.

(9) Asahi, R.; Morikawa, T.; Ohwaki, T.; Aoki, K.; Taga, Y. *Science* **2001**, 293, 269-271.

(10) Yin, M.; Wu, C. K.; Lon, Y. B.; Burda, C.; Koberstein, J. T.; Zhu, Y. M.; ÓBrien, S. *J. Am. Chem. Soc.* **2005**, 127, 9506-9511.

(11) Song, W.-S.; Yang, H. *Chem. Mater.* **2012**, 24, 1961−1967.

(12) Hameed, A.; Montini, T.; Gamboa, V.; Fornasiero, P. *J. Am.Chem. Soc.* **2008**, 130, 9658-9659.

(13) Kamat, P. V. *J. Phys. Chem. C* **2007**, 111, 2834-2860.

(14) Gupta, S. M.; Tripathi, M. *High Energy Chem.* **2012**, 46, 1−9.

(15) Wu, L.; Yu, J. C.; Fu, X. Z. *J. Mol. Catal.* **2006**, 244, 25-32.

(16) Li, G. S.; Zhang, D. Q.; Yu, J. C. *Environ. Sci. Technol.* **2009**, 43, 7079-7085.

(17) Xie, Y.; Ali, G.; Yoo, S. H.; Cho, S. O. *ACS Appl. Mater. Interfaces* **2010**, 2, 2910-2914.

(18) Xia, Y.; Tang, Z. *Chem. Comm.* **2012**, 48, 6320−6336.

(19) Li, J. T.; Hoffmann, M. W. G.; Shen, H.; Fabrega, C.; Prades, J. D.; Andreu, T.; Ramirez, F. H.; Mathur, S. *J. Mater. Chem.* **2012**, 22, 20472-20476.

(20) Jang, J. S.; Choi, S. H.; Kim, H. G.; Lee, J. S. *J. Phys. Chem. C* **2008**, 112, 17200-17205.

(21) Park, H.; Choi, W. Y.; Hoffmann, M. R. *J. Mater. Chem.* **2008**, 18, 2379-2385.

(22)Ye, M.; Gong, J. J.; Lai, Y. K.; Lin, C. J.; Lin, Z. Q. *J. Am. Chem. Soc.***2012**, 134, 15720-15723.

(23) Park, H.; Kim, Y. K.; Choi, W. *J. Phys. Chem. C* **2011**, 115, 6141-6148.

(24) Reber, J. F.; Rusek, M. *J. Phys. Chem.* **1986**, 90, 824-834.

(25) Wu, X. F.; Song, H. Y.; Yoon, J. M.; Yu, Y. T.; Chen, Y. F. *Langmuir* **2009**, 25, 6438-6447.

(26) Zhang, N.; Liu, S. Q.; Fu, X. Z.; Xu, Y. J. *J. Phys. Chem. C* **2011**, 115, 9136-9145.

(27) Baker, D. R.; Kamat, P. V. *Adv. Funct. Mater.* **2009**, 19, 805-811.

(28) Cao, S. W.; Yin, Z.; Barber, J.; Boey, F.; Loo, S. C. J.; Xue, C. *ACS Appl. Mater. Interfaces* **2012**, 4, 418-423.

(29) Tada, H.; Mitsui, T.; Kiyonaga, T.; Akita, T.; Tanaka, K. *Nat. Mater.* **2006**, 5, 782-786.

(30) Kelly, K. L.; Coronado, E.; Zhao, L. L.; Schatz, G. C. *J. Phys. Chem. B* **2003**, 107, 668-677.

(31) Silva, C. G.; Juárez, R.; Marino, T.; Molinari, R.; García, H. *J. Am. Chem. Soc.* **2011**, 133, 595-602.